Path-integral Monte Carlo study of the neon liquid-vapor interface

J. Q. Broughton
Complex Systems Theory Branch, Naval Research Laboratory, Washington, D.C. 20375-5000 and Sachs/Freeman Associates, Inc., Landover, Maryland 20785

Farid F. Abraham and J. A. Barker
IBM Research Division, Almaden Research Center, 650 Harry Road, San Jose, California 95120-6099
(Received 3 January 1989)

The neon liquid-vapor interface was studied at the triple point by path-integral Monte Carlo simulation with a view to determining the magnitude of quantum effects. Comparison is made between classical and quantum descriptions. The quantum interface is found to be approximately one quarter of an interatomic spacing wider than the classical counterpart. The surface tension is 20% lower than that obtained classically. Kinetic energy density profiles through the interface show anisotropy between the x and z directions. Marked differences are also found between the zero-pressure densities of the quantum and classical bulk liquid phases.

I. INTRODUCTION

Recently, calorimetric experiments on neon and argon multilayer films on graphite substrates have examined the interface width between crystal and melt.[1] The interface width was found to be six layers for neon and four for argon at their respective triple points. Since both systems may be described by the same reduced potential (that of Lennard-Jones) and because the principle of corresponding states[2] applies to these systems, we may conclude that quantum effects for the lighter element are the reason for this difference. The thermal de Broglie wavelength for the two systems (^{20}Ne and ^{40}Ar) at their respective triple points (24.56 and 83.81 K) are 0.31 and 0.12 Å to be compared with typical interatomic spacings in the liquid of 2.9 and 3.6 Å.[3]

Path-integral Monte Carlo simulations show significant differences to be present in the radial distribution functions of liquid neon treated classically and quantum mechanically at 35 and 40 K;[4] i.e., at temperatures in excess of the triple point. Further, the pair-correlation function for neon at the triple point, obtained directly from the pair-density matrix, shows very large differences between the quantum mechanical and classical descriptions.[5]

As an exploratory step towards the study of the crystal-melt system, we chose to investigate the liquid-vapor interface of neon at the experimental triple point of 24.56 K. The interface profile and surface tension of classical inert-gas liquid-vapor systems, as described by the Lennard-Jones potential have been extensively studied by Lee, Barker, and Pound[6] and by Miyazaki, Barker, and Pound.[7] The former used direct Monte Carlo simulation and integration of the virial through the interface to obtain the surface tension. The latter evaluated the same quantity in a statistically more accurate manner by reversibly cleaving the liquid. They obtained a value of 18.3 dyn/cm to be compared with an experimental value of 13.4 for argon. The difference is due mainly to three-body effects and inclusion of such through the Axilrod-Teller expression[8] brings simulation and experiment into close agreement.

We chose to employ path-integral Monte Carlo simulation to study neon using a propagator generated from the Lennard-Jones (LJ) potential by matrix squaring and employing the pair-product and end-point approximations.[9] Since neon at its triple point is still a distinguishable particle system and because it is not as quantum a fluid as liquid helium at 3 or 4 K, these approximations should be extremely good. We performed an intercomparative study of the ^{20}Ne liquid-vapor interface described classically and quantum mechanically at 24.56 K. Also, we investigated the ability of a quantum effective potential to describe the fully quantum-mechanical system.

Path-integral simulations are beginning to have an impressive record of describing interesting physics problems, such as the solvated electron,[10–14] solvated light atoms,[15] Bose condensation,[16] and incommensurate transitions of helium on graphite.[17] The method is particularly suitable for the system of interest here and special techniques have been employed to enable the investigation of the large system sizes necessary for interface simulation. We handle here 729 neon atoms.

In Sec. II we describe our system and algorithm. In Sec. III we give our results as well as expressions for the quantities calculated. We have, for example, three independent ways of evaluating the kinetic energy in the system. Finally, Sec. IV presents our conclusions.

II. SYSTEM AND ALGORITHM

A. System

The system comprised 729 atoms in the form of a slab periodically replicated in all three dimensions. The atoms interact via a Lennard-Jones potential (ϕ_{LJ}) parametrized for ^{20}Ne and truncated at $R_c = 2.5\sigma$ (see Fig. 1)

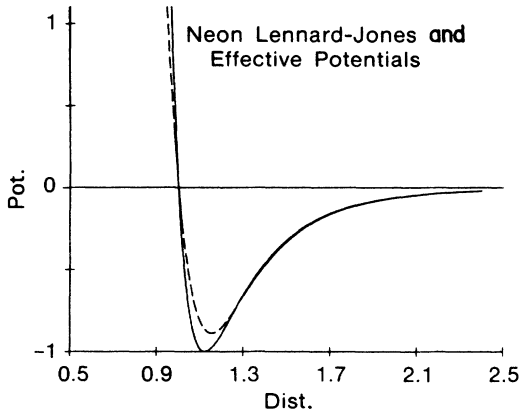

FIG. 1. Lennard-Jones (solid line) and effective potentials (dashed line) as $T=0.6855$ (24.56 K) vs distance. Reduced units are used.

$$\phi_{\mathrm{LJ}}=4\varepsilon\left[\left[\frac{\sigma}{r}\right]^{12}-\left[\frac{\sigma}{r}\right]^{6}\right] . \tag{1}$$

While such truncation in bulk systems at fixed density has negligible effect on atomic distribution functions, in interfacial simulations, correction for this truncation leads to a long-ranged time-independent force which may be handled through the use of an external mean-field potential

$$\phi_{\mathrm{ext}}=-\frac{4\pi\varepsilon\sigma^{6}}{2}\rho_0[I_1+I_2+I_3] , \tag{2}$$

where

$$I_1=\frac{1}{R_c^4}\max\{[\min(z+R_c,a)-\max(z-R_c,-a)],0\} ,$$

$$I_2=\begin{cases}\frac{1}{3}\left[\dfrac{1}{(z+a)^3}-\dfrac{1}{(z-\min\{z-R_c,a\})^3}\right], & z>R_c-a\\ 0, \quad \text{otherwise}\end{cases}$$

and

$$I_3=\begin{cases}-\frac{1}{3}\left[\dfrac{1}{(\max\{-a,z+R_c\}-z)^3}-\dfrac{1}{(a-z)^3}\right], & z<a-R_c\\ 0, \quad \text{otherwise} .\end{cases}$$

This correction assumes the liquid slab to be a rectangular parallelepiped with the faces normal to the z axis and bounded by the planes $z=\pm a$. These equations are valid for $-a-R_c\le z\le a+R_c$.

We report, as usual, all quantities in reduced units: that is, in units of σ, ε, m, and k. Unlike in classical mechanics, however, time-independent properties are mass dependent in quantum mechanics and we quote the values of ε, σ, and m used here ($\varepsilon/k=35.8$ K, $\sigma=2.75$ Å, and $m=19.9925$ amu).

The liquid-vapor classical system was equilibrated by heating a truncated face-centered-cubic (fcc) slab with a cross-sectional area of approximately $90\sigma^2$ at a temperature T of 1.00 for 50 000 Metropolis Monte Carlo moves (where one move represents N attempted displacements, N being the number of atoms in the system) before cooling to $T=0.685$ for 100 000 moves. Statistics were gathered over the next 100 000 iterations and the final configuration used as input to the path-integral and effective-potential Monte Carlo simulations. The effective-potential simulation was run a further 50 000 moves before gathering statistics over 100 000 moves while the path-integral simulations involved 30 000 moves equilibration and 30 000 moves for gathering statistics.

B. Algorithm

Path-integral Monte Carlo simulation is based upon Feynman's formulation of quantum mechanics.[18] The density matrix K of an N-particle system at temperature T is given by

$$K(\bar{R},\bar{R}';\beta)=\sum_i \psi_i(\bar{R})\psi_i^*(\bar{R}')e^{-\beta E_i} , \tag{3}$$

where i labels states of the system, ψ are the eigenfunctions, E is the energy, and β is $(1/kT)$. $\bar{R}$ refers to the $3N$ particle coordinates. All static properties of the system are obtainable from the density matrix which satisfies the identity

$$K(\bar{R},\bar{R}';\beta)=\int\cdots\int d\bar{R}_1\cdots d\bar{R}_{M-1}K(\bar{R},\bar{R}_1;\tau)\cdots K(\bar{R}_{M-1},\bar{R}';\tau) , \tag{4}$$

where $\tau=\beta/M$ and M can be any integer. $K(\tau)$ is the density matrix at the higher temperature MT. This multidimensional integral can be treated by the Monte Carlo method if the integrand is known. When M is sufficiently large, $K(\tau)$ can be approximated by its classical form

$$K(\bar{R},\bar{R}';\tau)=K^0(\bar{R},\bar{R}';\tau)\times\exp\left[-\frac{\tau}{2}[V(\bar{R})+V(\bar{R}')]\right] , \tag{5}$$

where K^0 is the free-particle density matrix

$$K^0(\bar{R},\bar{R}';\tau)=(m/2\pi\tau\hbar^2)^{-3/2}\exp\left[-\frac{m(\bar{R}-\bar{R}')^2}{2\tau\hbar^2}\right] . \tag{6}$$

In this so-called primitive algorithm each quantum particle is represented as a necklace of M classical beads in which each bead interacts with only its nearest neighbors

via a harmonic potential (which depends upon temperature) and with a reduced external field of $V(R)/M$. It is therefore possible to implement Monte Carlo importance sampling algorithms (we used the Metropolis scheme) to treat quantum many-body systems via a classical analog. The necklace analogy makes it clear that these (distinguishable) quantum systems are M times more computationally burdensome than the equivalent classical systems.

One way to reduce the number of beads is to use the quantum effective-potential instead of the classical potential in the high-temperature approximation [Eq. (5)]. The matrix-squaring method, which is an accurate and efficient method for obtaining the two-body density matrix, provides the means to produce an effective potential from the diagonal terms of the density matrix. The off-diagonal terms and the property estimators may be obtained from those on the diagonal via the end-point approximation. The entire density matrix may then be constructed using the pair-product approximation

$$K(\bar{R},\bar{R}';\beta)=\prod_{i=1}^{N} K^0(\bar{r}_i,\bar{r}_i';\beta)\prod_{\substack{i,j\\ i\neq j}}^{N}\tilde{K}(\bar{r}_{ij},\bar{r}_{ij}';\beta) \tag{7}$$

where $\bar{r}$ represents atomic coordinates and $\tilde{K}$ represents the normalized pair-density matrix

$$\tilde{K}(\bar{r}_{ij},\bar{r}_{ij}';\beta)=K(\bar{r}_{ij},\bar{r}_{ij}';\beta)/K^0(\bar{r}_{ij},\bar{r}_{ij}';\beta)\ . \tag{8}$$

The idea, then, is to use matrix squaring down to a temperature $T_{\rm med}$ at which the pair-product approximation is good and then, using the contents of the resulting density matrices, to employ Monte Carlo simulation to take us to the temperature of interest $T_{\rm fin}$. In this simulation we used ten beads. Hence $T_{\rm med}=6.855$ (or 245.6 K).

The matrix-squaring method follows directly from Eq. (4) which is exact. The two-body density matrix at temperature T can be obtained by numerical multiplication of the two identical density matrices representative of twice T

$$K(r,r';\beta)=\int d\mathbf{r}_1 K(\bar{r},\bar{r}_1;\beta/2)K(\bar{r}_1,\bar{r}';\beta/2)\ . \tag{9}$$

Starting at high temperature $T_{\rm high}$ at which K may be approximated by its classical expression [i.e., akin to Eq. (5)], after p iterations of matrix squaring, we end up with the density matrix for the lowest temperature $T_{\rm high}/2^p$. Larger and larger values of p were tried until the resulting density matrices at $T_{\rm med}$ became invariant. We found $p=10$ gave good results. The diagonal terms of the normalized pair-density matrix [Eq. (8)] are used as effective-potential terms in the propagator [Eq. (5)]. The consequence of using such a propagator is that only beads of like number (i.e., of like imaginary time) on neighboring necklaces interact. Hence we keep Verlet[19] (neighbor) lists for each imaginary time slice. These lists are updated via the cell method of Quentrec and Brot[20] approximately every ten Monte Carlo moves. It is this feature of the code that enables the treatment of large system sizes. The external potential which takes account of the 2.5σ truncation error is treated via the primitive algorithm [Eq. (5)]. We expect this approximation to be good because the external field varies slowly in space.

Turning now to the estimator matrices and noting that the total energy of a system is given by

$$E^{\rm tot}=-\frac{1}{Z}\frac{dZ}{d\beta}\ , \tag{10}$$

where Z is the partition function obtained from the diagonal terms of Eq. (3) and the kinetic energy is given by

$$E^{\rm kin}=\frac{m}{\beta Z}\frac{dZ}{dm}\ , \tag{11}$$

we define the following total-energy-estimator matrix:

$$M^{\rm tot}(\bar{r},\bar{r}';\beta)=\frac{dK(\bar{r},\bar{r}';\beta)}{d\beta}\ , \tag{12}$$

and kinetic-energy-estimator matrix:

$$M^{\rm kin}(\bar{r},\bar{r}';\beta)=\frac{dK(\bar{r},\bar{r}';\beta)}{dm}\ . \tag{13}$$

These estimator matrices (M) satisfy

$$M(\bar{r},\bar{r}';\beta)=\tfrac{1}{2}\int d\bar{r}_1[M(\bar{r},\bar{r}_1;\beta/2)K(\bar{r}_1,\bar{r}';\beta/2)+K(\bar{r},\bar{r}_1;\beta/2)M(\bar{r}_1,\bar{r}';\beta/2)]\ . \tag{14}$$

Again, in determining system properties, only diagonal terms are used in the estimator matrices.

In order to simplify the calculations, the three-dimensional density matrix can be reduced to a sum of one-dimensional matrices by the following partial-wave expansion:

$$K(\bar{r},\bar{r}',\beta)=\sum_{l=0}^{\infty}\frac{2l+1}{4\pi rr'}k_l(r,r';\beta)P_l(\cos\theta)\ , \tag{15}$$

where θ is the angle between $\bar{r}$ and $\bar{r}'$ and $P_l(x)$ are Legendre polynomials. Each k_l obeys analogous matrix-squaring relationships to Eq. (9) as do the l partial-wave expansions for the energy estimators.

The potential-energy estimator is obtained as the simple ensemble average of the potential energy between particles in the system. Thus we have independent methods for obtaining potential $E^{\rm pot}$, kinetic, and total energies and are able to determine internal consistency between the values of all three.

In actuality, we have a further check on the kinetic energy which comes from the expression[21] for the pressure components in the system necessary to calculate the surface tension (γ)

$$\gamma=\frac{1}{A}\left\{2\,\mathrm{tr}\left[-\frac{\hbar^2}{2m}\sum_{i=1}^{N}\left[\frac{\partial^2}{\partial z_i^2}-\frac{\partial^2}{\partial x_i^2}\right]\rho(r_1,\ldots,r_N;r_1',\ldots,r_N')\right](\mathrm{tr}\rho)^{-1}+\left\langle\sum_{i,j}\frac{x_{ij}^2-z_{ij}^2}{r_{ij}}\frac{\partial\phi}{dr_{ij}}\right\rangle\right\}\ . \tag{16}$$

After some manipulations this may be shown to be

$$\gamma=\frac{1}{A}\left[2(\langle E_z^{\rm kin}\rangle-\langle E_x^{\rm kin}\rangle)+\frac{1}{M}\left\langle\sum_{i,j}\sum_{p}\left[\frac{x_{ij}^2(p)-z_{ij}^2(p)}{r_{ij}(p)}\right]\frac{\partial\phi}{dr}\right\rangle\right], \tag{17}$$

where A is the surface area, M is the number of beads, p is the bead index, and x represents the average of the x and y components (i.e., the z direction is normal to the surface). This expression for the surface tension is identical to the classical analog derived from the virial except that now the kinetic energy terms are no longer simply $(kT/2)$ but are given by

$$\langle E_x^{\rm kin}\rangle=\frac{MNkT}{2}+\frac{1}{M}\left\langle\sum_{i=1}^{N}\sum_{p=1}^{M}\left\{\frac{\lambda}{4}\sum_{\substack{j\\ j\neq i}}\left[\frac{\partial^2\rho}{\partial r^2}[r_{ij}(p)]\frac{x_{ij}^2(p)}{r_{ij}^2(p)}+\frac{\partial\rho}{\partial r}[r_{ij}(p)]\left[\frac{1}{r_{ij}(p)}-\frac{x_{ij}^2(p)}{r_{ij}^3(p)}\right]\right]\right.\right.$$
$$-\frac{1}{2\lambda\tau^2}[x_i(p)-x_i(p+1)]^2-\left[\frac{1}{2\tau}[x_i(p)-x_i(p+1)]\sum_{\substack{j\\ j\neq i}}\frac{\partial\rho}{\partial r}[r_{ij}(p)]\frac{x_{ij}(p)}{r_{ij}(p)}\right]$$
$$\left.\left.-\frac{\lambda}{8}\left[\sum_{\substack{j\\ j\neq i}}\frac{\partial\rho}{\partial r}[r_{ij}(p)]\frac{x_{ij}(p)}{r_{ij}(p)}\right]^2\right\}\right\rangle \tag{18}$$

where $\lambda=\hbar^2/m$. The derivatives of ρ with respect to r are obtained by numerical differentiation of the diagonal terms of the pair density matrix at $T_{\rm med}$. Kinetic energy profiles $[E^{\rm kin}(z)]$ are obtained through the system by apportioning contributions from each pair interaction, half to one bead and half to the other.

The surface tension in the system may be obtained from the relationship

$$\gamma=\int[P_{zz}(z)-P_{xx}(z)]dz \tag{19}$$

where $P_{\alpha\alpha}$ is the $\alpha\alpha$ component of the pressure tensor.

Finally, for the effective-potential calculation, we matrix square all the way down to $T_{\rm fin}=24.56$ K and use the diagonal terms of the pair-density matrix so produced as the potential in a propagator for which there is only one bead. System properties are obtained from path-integral equivalents reduced similarly to one bead.

III. RESULTS

As in all Monte Carlo simulations, it is important to determine whether the system has equilibrated. Classical simulations on three-dimensional (3D) interfaces are now sufficiently routine that common experience indicates that a 100 000 move setup followed by 100 000 move statistics accumulation should provide accurate energies, densities, and surface tensions. However, for path-integral systems, it is not clear what typical equilibration periods might be. After the initial 30 000 move setup, the results indicated in Fig. 2, for kinetic, potential, and total energy per atom were obtained. The figure represents data acquired over a further 30 000 moves. These properties are seen to be very stable. The average kinetic energy of 1.3450 is obtained from Eq. (11). The kinetic energy obtained by difference from the total and potential energies is 1.397: the discrepancy between the two values, we feel, being caused by noninclusion of off-diagonal terms in the kinetic-energy-estimator matrix.[22]

Figure 3 illustrates the variation in x and z pressure components with the number of Monte Carlo moves for the quantum system, the difference between the two, suitably normalized, giving the surface tension. This is a

TABLE I. Comparison of system properties.

	Surface tension[a] ε/σ^2	Surface energy[a] ε/σ^2	Bulk density N/σ^3	Bulk energy ε/N
Classical	1.21±0.1	2.52±0.1	0.818	−5.943
Effective potential	1.01±0.1	2.54±0.1	0.773	−5.615
Quantum mechanical	1.01±0.3	2.33±0.2	0.770	−5.473

[a]rms deviation is included.

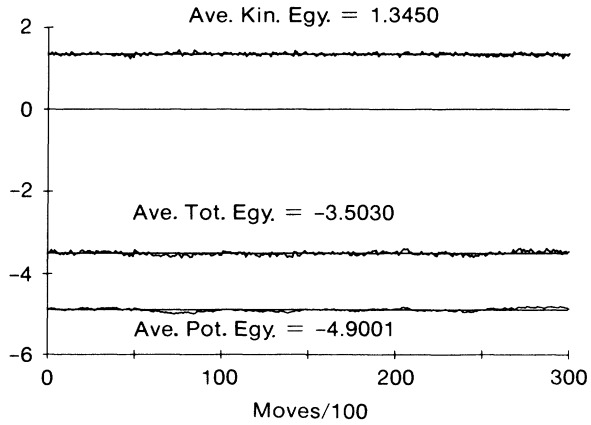

FIG. 2. Potential, kinetic, and total energies of the quantum neon surface system vs number of Monte Carlo moves. Reduced units are used.

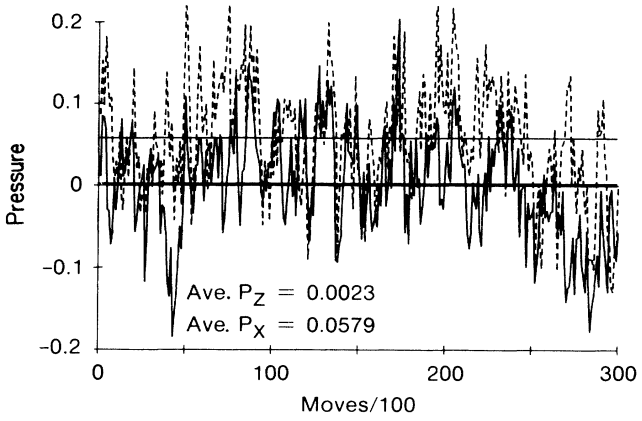

FIG. 3. Pressure in x (dashed) and z (solid) directions vs number of moves for the quantum neon surface. Reduced units are used.

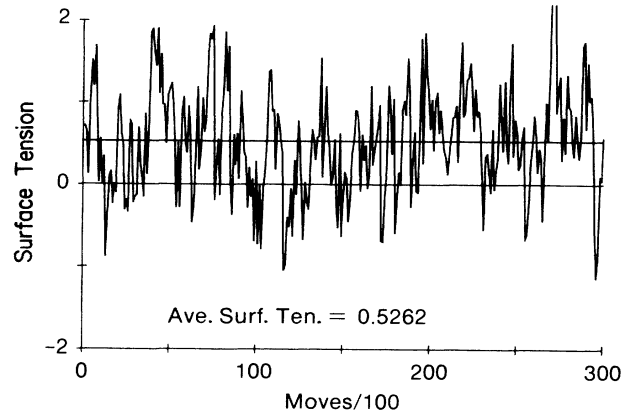

FIG. 4. Surface tension vs number of moves. Reduced units are used.

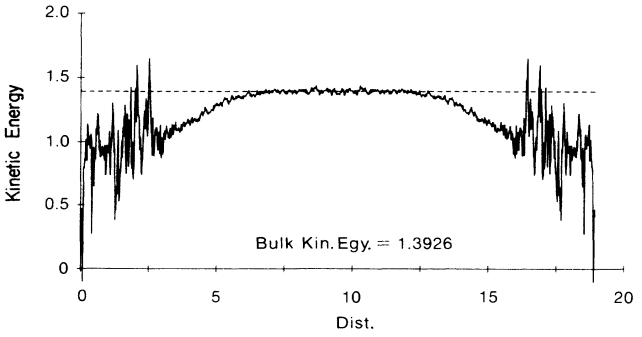

FIG. 5. Kinetic energy profile through the quantum neon surface, with over 30×10^3 quantum Monte Carlo moves. Reduced units are used.

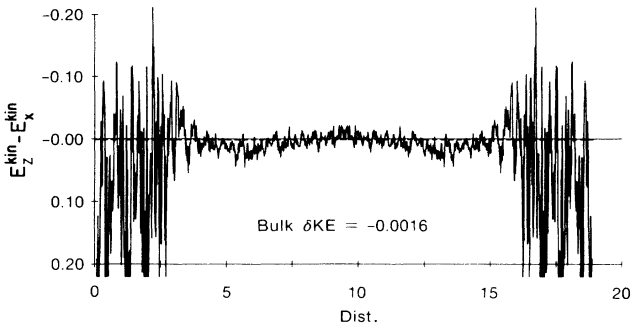

FIG. 6. Difference between x and z kinetic energies through the quantum neon surface, with over 30×10^3 quantum Monte Carlo moves. Reduced units are used.

noisy quantity. The average z pressure fluctuates around zero. The x pressure, on the other hand, is small and positive. For completeness, Fig. 4 gives the instantaneous value of the surface tension as a function of number of moves.

Inspection of Eq. (17) shows that the surface tension involves the difference of the x and z kinetic energies. This difference is extremely small and approximately 99% of the value of the surface tension comes from the virial contribution. Figure 5 plots the kinetic energy density profile (involving the sum of x, y, and z components) through the system. Note that the bulk value of 1.393 is significantly in excess of 1.028, the classical and free-particle value. Further note that the kinetic energy in the interfacial region drops and asymptotes (allowing for noise) to the free-particle value. The noise in the vapor region is caused by the very low density of particles here. Figure 6 shows the difference between x and z components of the kinetic energy. Notice, by comparison with Fig. 7(a) which gives the atom number density through the system, that as the density drops in going from the bulk through the interface, the x kinetic energy actually dominates that in the z. However, in the tails of the interface and out into the vapor, the kinetic energy becomes isotropic once more.

Table I presents results for the bulk densities and energies and the surface tensions and energies (actually potential energies) for the quantum, effective-potential, and classical systems. The classical system always produces quantities which are larger, in an absolute sense, than the quantum equivalent. The effective-potential system performs well at mimicking the full quantum-mechanical system and only fails for the excess energy calculation.

TABLE II. Full width at half height.

	Number-density profile	Potential-energy profile
Classical	8.02	10.24
Effective potential	8.50	10.87
Quantum mechanical	8.52	10.77

That the "one-bead" system performs so well indicates that the ten-bead simulation is a very accurate representation of the fully quantum-mechanical system. Our classical bulk density is lower than that found by Hansen and Verlet.[23] At the LJ triple point of 0.67 they found a density of 0.86. The quantum-mechanical density of 0.7698 (1.2289 g/cm^2) compares favorably with the experimental value of 1.248 g/cm^3. Our quantum-mechanical surface tension of 1.01 (6.60 dyn/cm) compares with an experimental value[2] of 5.61 dyn/cm. The difference is undoubtedly due to the absence of three-body terms in the description of the system.[6]

One of the motivations for this study was the interface width dependence of neon versus argon crystal-liquid systems. We ask the question whether this interface width difference is also present in the liquid-vapor system. Fig-

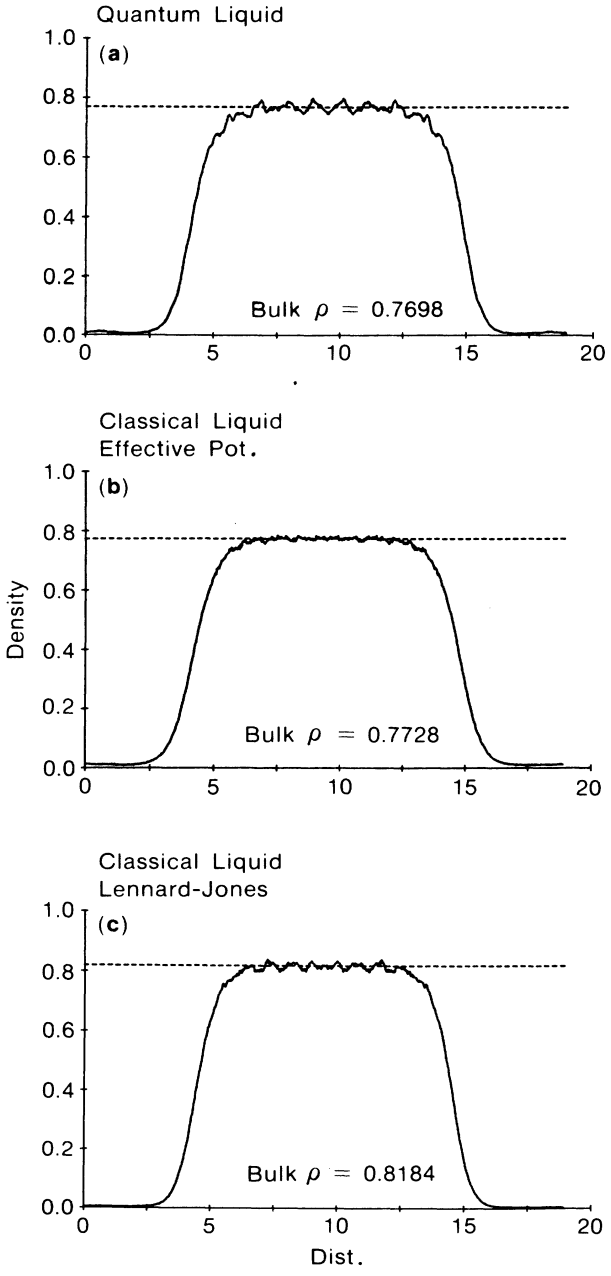

FIG. 7. Number density profiles through system. (a) Quantum mechanical, (b) effective potential, (c) classical. Reduced units are used.

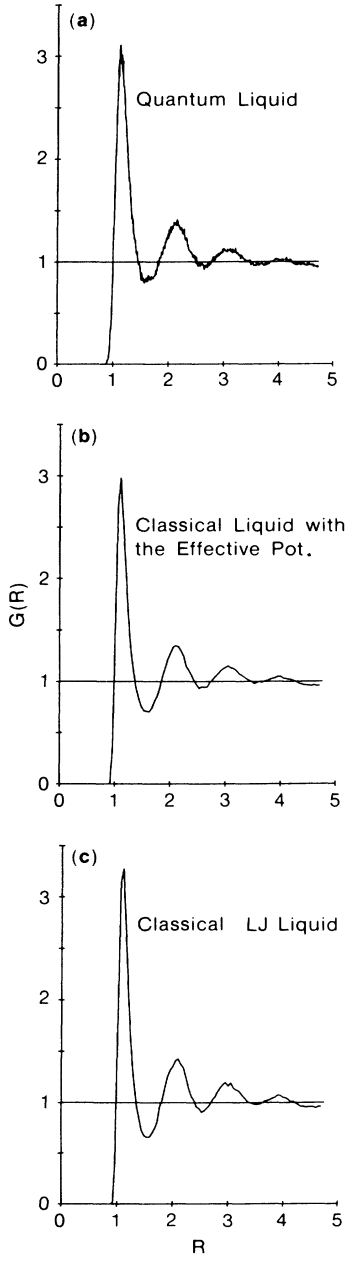

FIG. 8. Radial distribution functions in the center of the slab. (a) Quantum mechanical, (b) effective potential, (c) classical. Reduced units are used.

ures 7(b) and 7(c) give the density profiles of the classical and effective-potential systems. Differences are difficult to determine by eye; but a useful quantity, given that each system comprises 729 atoms, is the full width at half height of the density profile. Table II gives this quantity for the number density as well as the potential-energy density profiles. The quantum-mechanical system has an interface, as determined by either of the two profiles, which is approximately 0.25σ broader per face than the classical equivalent. Further, the effective-potential calculation mirrors the full path-integral calculation closely. There is, therefore, a small but discernible difference between the interface widths of the classical and quantum-mechanical systems, but nothing like the two-layer difference found experimentally for crystal-liquid interfaces.[1]

Finally, we compare in Fig. 8 the bulk (i.e., obtained from the center of the slab) radial distribution functions of the three systems. The first peak is lower for the quantum-mechanical and effective-potential calculations than that of the purely classical system. Further, the first peak of the quantum system is broader than those of either the effective-potential or classical systems. The dissimilarities between the bulk distribution functions of the three systems, however, are not large. This observation is in accord with the results of Thirumalai, Hall, and Berne[4] at the slightly higher temperatures of 35 and 40 K, but lower densities of 0.66 and 0.68, respectively, who found relatively small differences between the radial distribution functions of classical and quantum-mechanical bulk neon.

IV. CONCLUSIONS

We have performed an intercomparative study of the liquid-vapor interface of neon at the experimental triple point described both classically and quantum mechanically. The effect of quantum corrections is to lower the bulk zero-pressure density and also the surface tension. The kinetic energy profile shows that the x and z components become anisotropic at the point at which the density starts to drop away from the bulk value. At the point of inflection in the interface density profile and out towards the vapor, the kinetic energy returns to being isotropic. Finally, we find that although the radial distribution functions of the bulk quantum and classical liquids are very similar, the interface widths are different. In fact, we find that the quantum interface is approximately a quarter of an interatomic spacing wider than the classical equivalent.

[1]D-M. Zhu and J. G. Dash, Phys. Rev. Lett. **60**, 432 (1888).
[2]E. A. Guggenheim, J. Chem. Phys. **13**, 253 (1945).
[3]G. L. Pollack, Rev. Mod. Phys. **36**, 748 (1964).
[4]D. T. Thirumalai, R. W. Hall, and B. J. Berne, J. Chem. Phys. **81**, 2523 (1984).
[5]A. D. Klemm and R. G. Storer, Aust. J. Phys. **26**, 43 (1973).
[6]J. K. Lee, J. A. Barker, and G. M. Pound, J. Chem. Phys. **60**, 1976 (1974).
[7]J. Miyazaki, J. A. Barker, and G. M. Pound, J. Chem. Phys. **84**, 3364 (1976).
[8]J. A. Barker, R. A. Fisher, and R. O. Watts, Mol. Phys. **21**, 657 (1971).
[9]E. M. Pollock and D. M. Ceperley, Phys. Rev. B **30**, 2555 (1984).
[10]M. Parrinello and A. Rahman, J. Chem. Phys. **80**, 860 (1984).
[11]C. D. Jonach, C. Romero, and A. Rahman, Chem. Phys. Lett. **123**, 209 (1986).
[12]U. Landman, D. Scharf, and J. Jortner, **54**, 1860 (1985).
[13]J. Bartholomew, R. W. Hall, and B. J. Berne, Phys. Rev. B **32**, 548 (1985).
[14]M. Sprik, M. L. Klein, and D. Chandler, Phys. Rev. B **32**, 545 (1985).
[15]B. De Raedt, M. Sprik, and M. L. Klein, J. Chem. Phys. **80**, 5719 (1984).
[16]D. M. Ceperley and E. M. Pollock, Phys. Rev. Lett. **56**, 351 (1986).
[17]F. F. Abraham and J. Q. Broughton, Phys. Rev. Lett. **59**, 64 (1987).
[18]R. P. Feynman and A. R. Hibbs, *Quantum Mechanics and Path Integrals* (McGraw-Hill, New York, 1965).
[19]L. Verlet, Phys. Rev. **159**, 98 (1967).
[20]B. Quentrec and C. Brot, J. Comp. Phys. **1**, 430 (1973).
[21]S. Ono and S. Kondo, in *Structures of Liquids*, Vol. 10 of *Handbüch der Physik*, edited by S. Flügge (Springer-Verlag, Berlin, 1960), p. 240.
[22]E. L. Pollock (private communication). In order to calculate accurate kinetic energies, it is necessary to describe off-diagonal elements to higher order than is necessary for the propagator.
[23]J-P. Hansen and L. Verlet, Phys. Rev. **184**, 151 (1969).